Characterization of Seismicity from Different Glacial Bed Types: Machine Learning Classification of Laboratory Stick-Slip Acoustic Emissions

Seth Saltiel[1], Nathan Groebner[2], Theresa Sawi[3], Christine McCarthy[4], and Benjamin Kamine Holtzman[5]

[1]University of Nevada, Reno
[2]University of Minnesota
[3]Lamont-Doherty Earth Observatory
[4]Lamont-Doherty Earth Observatory, Columbia University
[5]Lamont-Doherty Earth Observatory, Columbia Univ.

February 27, 2023

Abstract

Subglacial seismicity provides the opportunity to monitor inaccessible glacial beds at the epicentral location and time. Glaciers can be underlain by rock or till, which determines the mechanics of slip and, if unstable, characteristics of resulting seismicity. Utilizing a double direct shear apparatus, we found conditions for instability at freezing temperatures and high slip rates for both bed types, although with very different frictional evolution. During stick-slip stress-drops, we recorded acoustic emissions with piezoelectric transducers frozen into the ice. Supervised machine learning can classify recorded waveforms and spectra as coming from rock or till beds. The Random Forest Classifier is interpretable, with the prediction based on the initial oscillation peaks and high frequency energy. Till events are generally higher stress-drop, with more impulsive first arrivals compared to rock waveforms. These seismic signatures of mechanical slip processes and associated bed conditions can potentially greatly enhance interpretation of subglacial seismic data.

Characterization of Seismicity from Different Glacial Bed Types: Machine Learning Classification of Laboratory Stick-Slip Acoustic Emissions

S. Saltiel[1], N. Groebner[2], T. Sawi[3], C. McCarthy[3], B.K. Holtzman[3]

[1]Nevada Seismological Laboratory, University of Nevada, Reno, NV, USA

[2]Strabo Analytics, Inc, New York, NY, USA.

[3]Lamont-Doherty Earth Observatory, Columbia University of New York, NY, USA

Corresponding author: Seth Saltiel (ssaltiel@unr.edu)

Key Points:

- Ice slip on frozen till or rock at high velocity produce stick-slip stress-drops with AEs recorded on transducers frozen into the ice
- Supervised machine learning can determine bed type (rock versus frozen till) from waveform or spectral features
- Feature importance shows till events are more impulsive/higher frequency, consistent with higher stress-drops, friction, and healing

Abstract

Subglacial seismicity provides the opportunity to monitor inaccessible glacial beds at the epicentral location and time. Glaciers can be underlain by rock or till, which determines the mechanics of slip and, if unstable, characteristics of resulting seismicity. Utilizing a double direct shear apparatus, we found conditions for instability at freezing temperatures and high slip rates for both bed types, although with very different frictional evolution. During stick-slip stress-drops, we recorded acoustic emissions with piezoelectric transducers frozen into the ice. Supervised machine learning can classify recorded waveforms and spectra as coming from rock or till beds. The Random Forest Classifier is interpretable, with the prediction based on the initial oscillation peaks and high frequency energy. Till events are generally higher stress-drop, with more impulsive first arrivals compared to rock waveforms. These seismic signatures of mechanical slip processes and associated bed conditions can potentially greatly enhance interpretation of subglacial seismic data.

Plain Language Summary

A glacier can lurch forward while slipping on its base, releasing seismic waves like an earthquake, which are monitored from the surface. Just like in a tectonic setting, only certain conditions allow for this type of motion, and aspects of the bed conditions affect how they slip and the resulting waves. We approximate glacial bed conditions in the lab of two very different types, soft (sediment) and hard (rock), and measure lurching behavior and resulting waves from each. Using a variety of data science techniques, we decipher subtle differences between the two bed types from remotely-sensed waves. This suggests that seismicity can provide important information on glacial bed conditions and how they differ in time and space.

1 Introduction

Future sea-level rise will largely be determined by fast-slipping polar glaciers, known as ice streams [Cuffey & Paterson 2010]. Since motion is mostly concentrated at their beds, conditions there have an outsized effect on the entire system's mass-balance and evolution. Glacial beds are separated, to first order, into hard bedrock or soft sediment (till), and then as either 'wet' (melting temperature) or 'dry' (frozen or drained) [Clarke 2005]. Water and sediment can flow and evolve on much shorter time scales than ice deforms, so the bed is one of the most dynamic parts of the ice sheet system, assumed to be responsible for recent changes in ice flow configurations [Bougamont et al., 2015] and ongoing responses to the changing climate [Parizek et al., 2013].

Although the basal system is difficult to directly access, growing observations of subglacial seismicity offer the opportunity to monitor changes with high temporal and spatial resolution [Aster & Winberry 2017]. Recent studies have used subglacial seismicity observations to infer differences in bed strength [Guerin et al., 2021], failure mechanism [Kufner et al., 2021], fine-scale asperity interactions [Gräff et al., 2021], basal water pressure [Gräff & Walter 2021], as well as local basal shear-stresses and slip-rates [Hudson et al., 2022].

Seismic observations are particularly useful since there are limited glacial bed conditions that have been shown to exhibit the requisite conditions for seismic failure [Iverson 2010, Lipovsky et al., 2019]. Classically, ice deformation, and thus slip due to regelation and viscous creep, is assumed to be rate-strengthening [Schoof 2005]. Till deformation was also first treated as viscous but later shown to be Coulomb plastic, essentially rate-neutral [Iverson 2010, Zoet & Iverson 2020]. But nucleation of seismic instability requires rate-weakening resistance, described by the rate-state stability parameter ($b - a$), which allows acceleration due to feedback with decreasing friction, as has been shown for fault rocks and gouge [Marone 1998]. This situation provides the opportunity for seismic observations to present a strong constraint on the conditions at their epicentral location and origin time, but each potential stick-slip mechanism and characteristics of resulting seismicity must be thoroughly understood to determine what conditions recorded seismic events represent.

Laboratory simulations provide the opportunity to directly observe slip behavior under controlled conditions. To date, seismically required rate-weakening has been reported for debris-laden ice on impermeable rock at sub-freezing temperature and permeable rock at the pressure melting point [Zoet et al., 2013], pure ice on impermeable rock at sub-freezing temperature [McCarthy et al., 2017], and pure ice on till at sub-freezing temperature [Saltiel et al., 2021], with stick-slip stress-drops reported for debris-laden ice on impermeable rock at sub-freezing temperature [Zoet et al., 2020]. These findings suggest that seismicity is largely associated with dry (frozen or drained) conditions. Although fast-slipping glaciers are commonly assumed to occur on wet, temperate beds, local mechanisms could freeze bed regions, for example around obstacles [Robin 1976]. Experiments have also shown rate-weakening is possible due to cavity formation behind hard bed obstacles [Zoet & Iverson 2016] and pore-pressure feedback from clast ploughing [Thomason & Iverson 2008]. Although each of these mechanisms, and the bed conditions which enable them, show rate-weakening drag, their frictional evolution can differ dramatically. For example, the critical slip distance (D_c) over which friction evolves to a new steady-state after a change in slip rate varies by more than an order of magnitude between rock and till beds under similar conditions in the same apparatus [McCarthy et al., 2017, Saltiel et al., 2021]. These mechanisms' different frictional characteristics and applicable scales likely contribute to aspects of the resulting seismicity, which could further constrain epicentral bed conditions.

We report here, for the first time, experimental stick-slip stress-drops for pure ice on impermeable rock and till at sub-freezing temperatures. In addition, we measured acoustic emissions (AEs) from these settings and analyze the measured waveforms using machine learning (ML) classification algorithms to find the characteristics associated with each bed type. By improving our understanding of the mechanisms of unstable slip in glacial settings and their expression in seismic emissions, these experiments and analysis techniques provide the opportunity to extract more information on conditions / source mechanics of subglacial or other seismic settings.

2 Experimental Methods and Materials

Experiments were conducted using an ambient pressure, cryogenic temperature, servo-hydraulic biaxial friction apparatus [McCarthy et al., 2016], with modifications to the insulating cryostat and loading procedure to allow measurement of till [Saltiel et al., 2021]. In this double-direct-shear configuration, a central ice block slides against two stationary side blocks, with layers of pre-compacted and frozen till or rock on opposite sides of the ice, such that applied horizontal load is resolved as normal stress and vertical load as shear stress on the sliding interfaces (Figure 1a). Additional experimental details are described in supporting text S1.

We made three additional modifications to the apparatus from Saltiel et al., [2021]. A Linear Variable Inductance Transducer (LVIT) position sensor measures the sample displacement separate from the loading point's preset displacement. This allowed measurement of displacement in each stress-drop 'slip' event as well as how much slip occurs during 'stuck' periods and the timing of both relative to stress-drops (Figure 1b). Here we refer only to mechanical or bulk stress-drops, the stress change during a slip event as measured by our vertical load cell, not to be confused with seismologically derived stress-drops. A rubber material was inserted into the loading geometry that effectively reduced the stiffness of the apparatus, reaching critical stiffness and allowing stick-slip instability [Zoet et al., 2020]. We estimate the effective apparatus stiffness using the mechanical data's reloading slope between stress-drops, relative to the compression of the loading train including rubber, the load point displacement minus sample displacement (Figure 1b). We estimate the apparatus stiffness after adding the rubber to be ~ 0.1 kPa/µm or ~ 5 x 10^5 N/m, significantly less stiff than was estimated without the rubber ~ 1 kPa/µm [Saltiel et al., 2021]. Additionally, commercial piezoelectric transducers were frozen into the central ice block, facing one of the ice-bed interfaces, to measure AEs. After experimenting with four different types of transducers of varying sizes and frequency sensitivities, we settled on Physical Acoustic's Nano-30™ miniature AE sensor due to its small size and 125-750 kHz response, covering the major frequency content of the events. All AEs analyzed here were recorded with a single Nano-30.

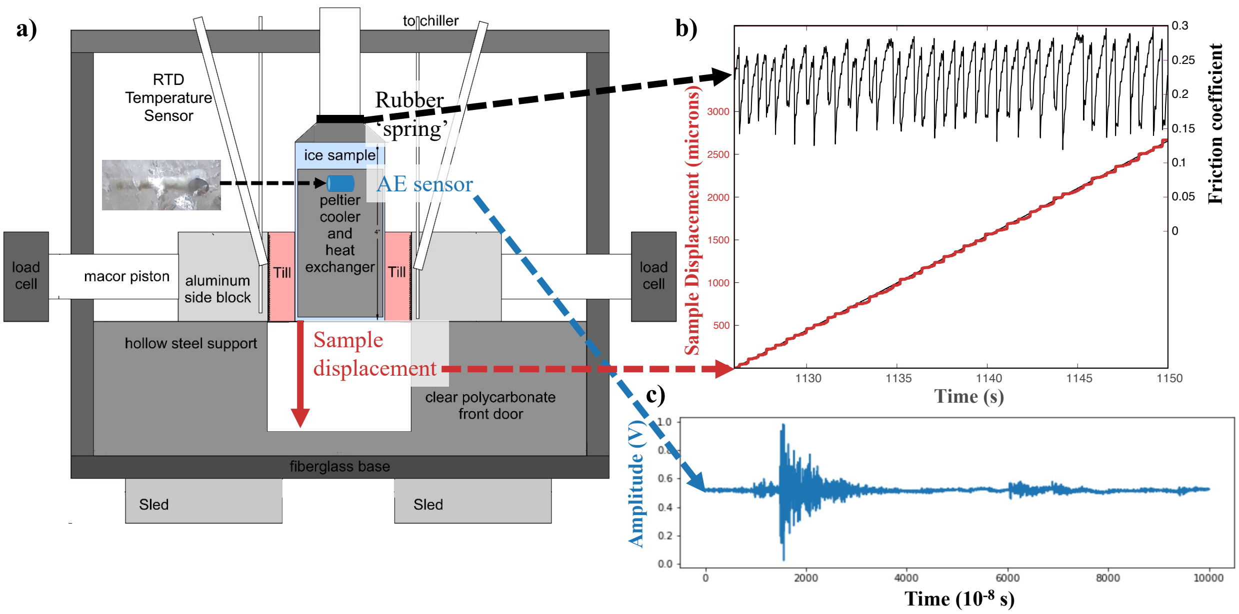

Figure 1: a) Schematic of biaxial cryostat with additions of rubber spring, to decrease loading stiffness, AE sensor frozen into central ice bock (pictured within ice in inset on left), and sample displacement measurement, modified from Saltiel et al., [2021]. For more details about apparatus see that publication and supporting text S1. **b)** An example experiment of measured friction drops (in black on top) and stick-slip sample displacement (in red on the bottom) with the steady load point displacement (in black) for reference. Instability was induced by apparatus reaching subcritical stiffness. **c)** An example AE waveform before processing, from a single stress-drop.

AEs were recorded using a preamplifier and TiePie™ HS6 differential digital oscilloscope. To ensure we recorded all relevant spectral content in the waveforms, they were recorded at a sample rate of 100 MHz for 1 ms time windows around each event (Figure 1c). These oscilloscope settings provided the optimal real-time viewing of waveforms as they were being recorded (see supporting movie S1 of experiment including audible stress-drops), but subsequent analysis showed most of the energy was under 1 MHz, and waveforms were down-sampled to 10 MHz and windowed to 15 µs. Recordings of continuous acoustic signal without applied shear found electrical noise above 3 MHz, so filtering also helped remove persistent noise sources. The oscilloscope was set in rising-limb trigger mode with trigger amplitude set just above the noise level before slip initiates, such that it did not trigger without an audible stress-drop. Since electrical and other sources of noise can vary, this trigger level was adjusted throughout the experiment to maximize the number of captured events and minimize waveforms of purely noise, but some events were missed, and some events triggered by noise or other AE sources were saved.

3 Data Processing and Machine Learning Analysis

Most events directly correspond to bulk mechanical stress drops, but to remove AEs associated with other types of sources (smaller patches of slip, cracking…), noisy events, non-events triggered by noise, and to normalize the waveforms in a way that focuses on the initial wave arrivals, we implemented a data cleaning and normalization approach based on that implemented by Nolte & Pyrak-Nolte [2022], described in supporting text S2.

After removing noisy waveforms, we end up with 2817 total events, including 1547 waveforms from 6 till experiments and 1270 waveforms from 6 rock experiments. With this labeled catalog (Figure 2), we systematically explored the ability of numerous supervised ML algorithms to predict the bed type for each event based on their waveform and spectra.

Input features to the machine learning models were the normalized waveform amplitudes at each timestep or the $\log_{10}$ power at each frequency for the spectra. The trained models select the most important temporal portions of the waveforms or frequencies in the spectra for discriminating between bed labels. We tested five basic ML classification algorithms including XGBoost (mean prediction accuracy ~74%), random forests (~77%), support vector machines (~75%), Naïve Bayes (~71%), K-nearest Neighbors (~76%), and fully connected neural networks (~75%). The waveforms and spectra were independently broken into train and test datasets. Hyperparameters were tuned for each algorithm and input data type (time or frequency domain) using 5-fold cross validation, and the highest-accuracy model for each algorithm was then used for prediction on the test set. The results of all our tests are summarized in supporting text S3, but here we focus our analysis on the Random Forest Classifier model [Breiman 2001] applied to the processed catalog, since it obtained some of our highest prediction accuracies, but, most importantly, it gives the feature importance needed to interpret how the model obtains its results. The feature importance shows the weighting of each waveform sample or frequency in making its prediction (Figures 4a and b). The feature importance is key for interpreting how the prediction is made and visually highlighting the subtle differences between different event sources. The purpose of this study is to understand how bed differences manifest in the resulting emissions, not to find a black-box algorithm which best differentiates them.

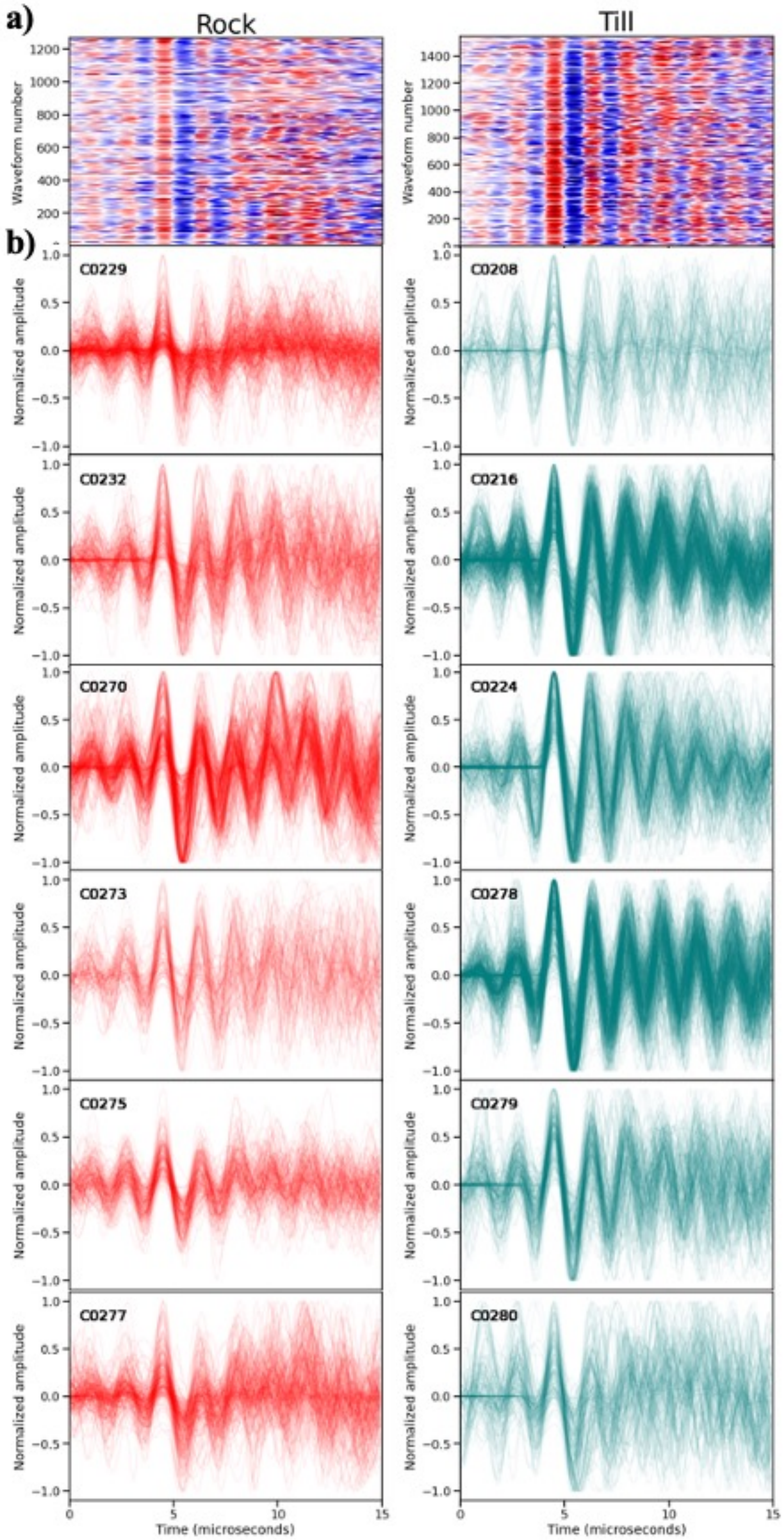

Figure 2: a) Waveforms plotted in chronological order along y-axis, colored by (normalized) amplitude (red is positive and blue negative). Rock events are plotted on the left and till on the right. **b)** Waveforms plotted together for each experiment (labelled on upper left). Each waveform (rock in red and till in teal) is plotted with a thin, light line, so the darker parts show many waveforms aligned on top of each other, and broader lines show less alignment. Since experiments vary significantly by number of events (94 – 465), that also contributes to the appearance of each experiment plot. Although there are subtle visual differences, it is not obvious that the two beds can be deciphered, making it a useful dataset to explore ML-based classification.

4 Stick-Slip Instability at Frozen Conditions

These experiments show the temperature dependence of instability, as both rock and till experiments were undertaken over a range of temperatures. Although analyzing the temperature dependence of AEs is outside of the scope of this letter, we did find stress-drops only at frozen temperatures (< ~ 0 °C for rock and < ~ -2.5 °C for till beds in Figure 3). It must be noted that temperatures are approximate, since they are measured behind the till/rock, there is some lag time before the temperature on the sliding interface reached those recorded. This is consistent with rate-weakening friction shown for till beds at ~ -3 °C using the same apparatus [Saltiel et al., 2021]. We estimate the apparatus stiffness with rubber to be ~ 0.1 kPa/μm or ~ 5 x 10^5 N/m, which is the same order of magnitude as the critical stiffness estimated from velocity-step experiments ~ 0.02 kPa/μm or 1 × 10^5 N/m (calculation on page 13 of Saltiel et al., [2021]). This factor of five difference is consistent with the error inherit in applying estimations of rate-state friction parameters ($b - a$, D_c) from a single experiment, as well as in our rough estimation of apparatus stiffness. Past studies of ice on rock friction did not find rate-weakening until lower temperatures, < ~ -18 °C for McCarthy et al., [2017]. In that study, experiments above -18 °C which exhibited slight rate-strengthening were undertaken at less than half the slip rate, which could affect the rate-dependence as well as stability more broadly [Schulson & Fortt 2012]. It is also possible to reach instability at nominally stable conditions given the strong elastic contrast between ice and rock beds [Rice et al., 2001]. This highlights the range of factors that contribute to seismic instability, further experiments and analysis are needed to fully map the conditional dependence of stability.

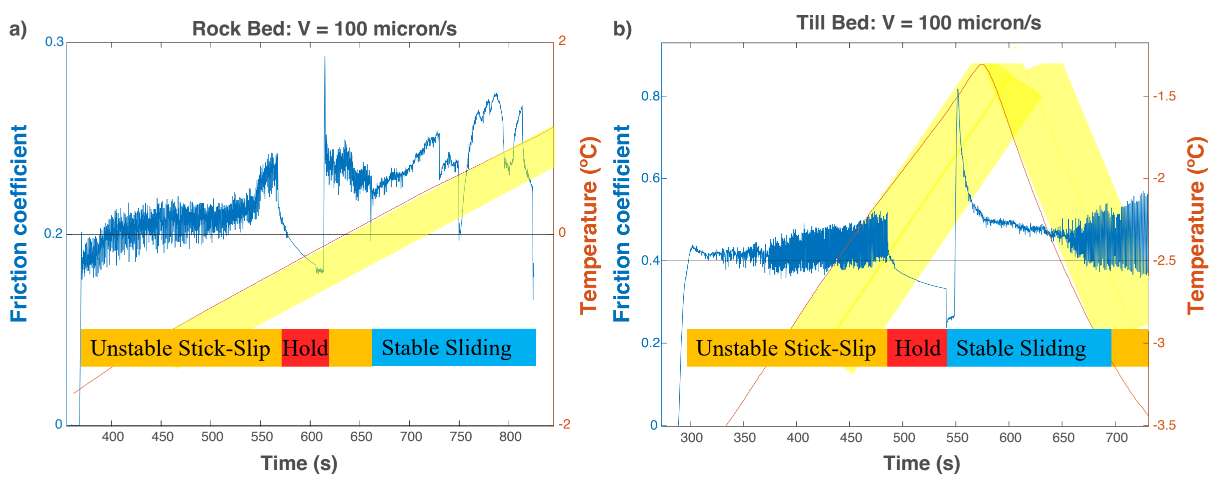

Figure 3: Example experiments of the temperature effect on slip stability for **a)** rock and **b)** till beds. Each experiment begins with stress-drops but, after a hold (described in supporting text S1), with increasing temperature the ice starts to slide stably without sudden friction drops or audible stick-slips. The transition to stable sliding occurs around 0 °C for the rock experiment. In the till experiment, the stability temperature is reached during the hold, but as it is re-cooled stress-drops resume below about -2.5 °C. Each estimated transition temperature is highlighted with a solid black horizontal line, but the temperatures are not measured directly at the ice-bed interface, so the interface temperature lags that recorded. The lag time (estimated to be ~100 s given rock/till thermal diffusivities ~1 mm^2/s) is represented by the yellow region right of the measured temperature. Additionally, when the temperature probe goes above ~0 °C the ice will remain at its

pressure melting point. It is also apparent that the till experiment has higher friction and healing rate (as the friction rose more after hold times of similar duration).

5 Bed Type Classification from Acoustic Emissions

Using a wide range of classification algorithms, we consistently find prediction accuracy above 50%, mostly between 65% and 80% (Supporting Figure S3), showing it is possible to tell if a population of AEs was emitted by a till or rock bed. This is not clear by visually examining the waveforms (Figure 2), showing algorithms successfully extract subtle features corresponding to the different bed labels. The logarithm of event spectra is also predictive (see supporting text S4).

To be able to apply our findings from laboratory AEs to field-scale seismicity, it is vital that we can interpret how the algorithms make their prediction. Although transfer learning methods offer the potential to train with labelled laboratory or modelled datasets and 'transfer' the model to more limited field or laboratory data [e.g., Wang et al., 2021], clear differences in the spectral content, travel path effects, and scale of field seismic data make this a daunting task. By isolating and interpreting the features the algorithms are using to make their successful predictions, we can understand the differences to look for and interpret in field data. The feature importance for the Random Forest Classifier model shows that it focuses on the peak and valley of the first full oscillation of the initial wave arrival (Figure 4a). Plotting all the normalized waveforms (color coded by bed type) together, we can see that the till (teal) waves tend to have higher amplitude in these first peaks. Similarly, log spectra show more energy at higher frequencies for the till in comparison to rock spectra (Figure 4b). Analyzing the mechanical data from 23 till and 22 rock experiments (including other experiments without recorded AEs), we find that the stress-drops of stick-slip events on till beds are generally higher (Figure 4c). The more impulsive arrivals and higher frequency content is consistent with till's higher stress-drops, since seismological stress-drop is calculated by the corner frequency where energy starts to fall off [e.g., Zoet et al., 2012]. This, in turn, can be explained by till's higher healing (Figures 3 and 4d), friction (Figure 3), as well as the rougher till surface (with its larger grain sizes).

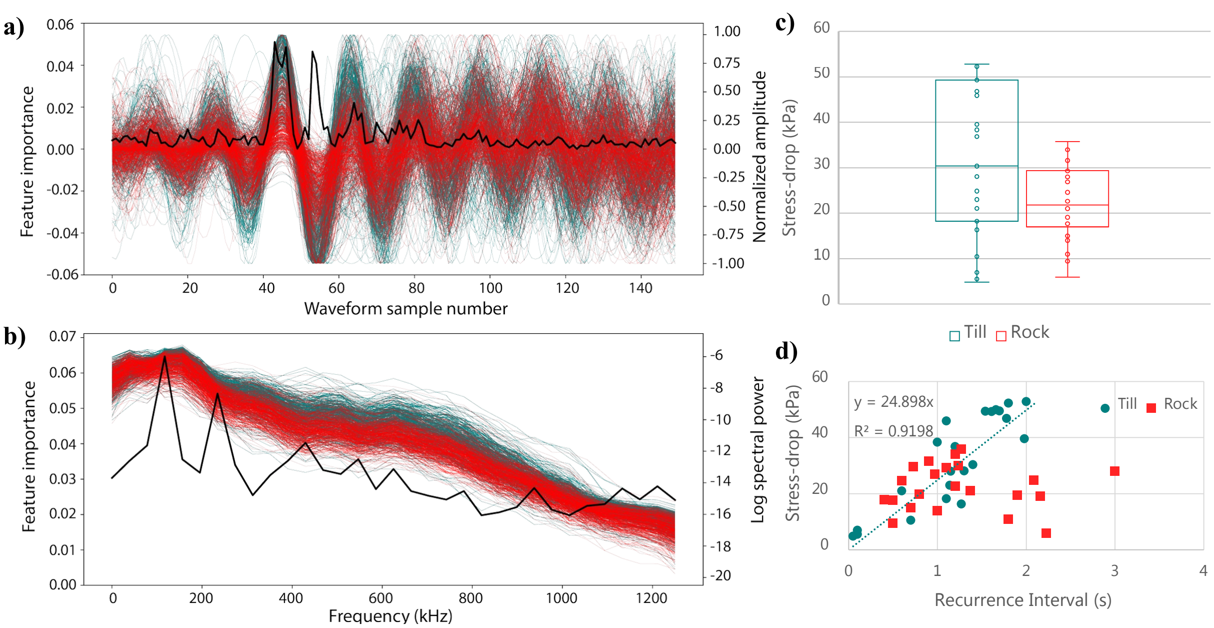

Figure 4: a) Feature importance, showing the weighting of each waveform sample to the model prediction, highlights the importance of the initial wave arrivals. The superimposed normalized

waveforms show till (teal) events are higher amplitude than rock (red) in these first oscillations. **b)** Feature importance of each frequency in the model prediction, show till (teal) and rock (red) spectra partially separate from each other above about 100 kHz, with till having more energy at these higher frequencies. **c)** Distribution of largest repeated mechanical stress-drop amplitude from 23 till and 22 rock experiments at similar conditions show till has higher stress-drops, although the two populations overlap significantly. **d)** Stress-drops vs recurrence interval for till and rock experiments shows till's greater healing (higher slope) contributes to higher stress-drops, while rock healing varies, but is generally lower.

It is likely that obtaining much higher prediction accuracies is impossible since each bed creates events like the other. The stress-drop and healing rates of the two populations clearly overlap (Figure 4c and d); spectra and waveform characteristics do as well. How this effects prediction can be most clearly seen with the log spectra since the visual separation is greatest. Figure 5a and b show that misclassified events are in the region between the event types, while Figure 5c shows that the waveform statistical attributes also greatly overlap. Although correctly predicting every event is unrealistic, given a sufficient sample size, our results suggest it could be possible to predict the bed type of a group of events from the same epicentral conditions (see supporting text S5).

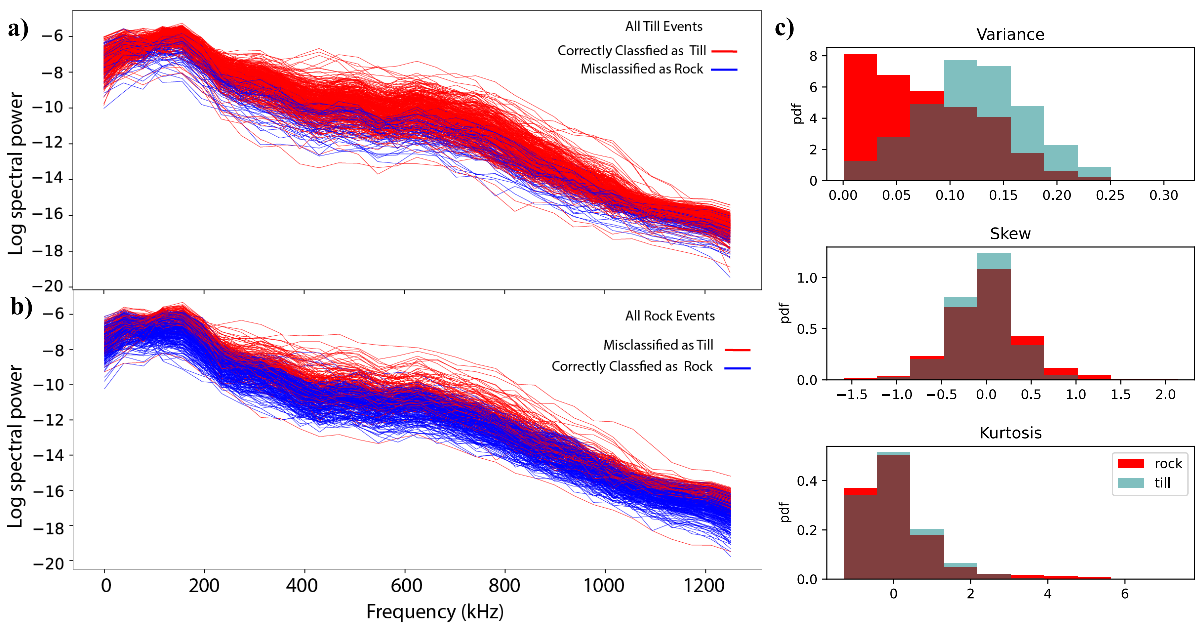

Figure 5: Log spectra of correct and misclassified **a)** till and **b)** rock events and **c)** distributions of statistical measures of waveforms from all experiments from each bed show how much the event populations overlap. The higher variance in the till waveform distributions is due to their more impulsive nature, but there are many rock events with just as high variance.

6 Conclusions

This study presents stick-slip stress-drops and resultant AEs for ice on rock and till beds at sub-freezing temperatures, a labeled dataset with which we explore how ML can decipher the bed from AE characteristics. We found that instability, and thus seismicity, only occurs for each bed below a certain temperature (~0 °C for rock and ~-2.5 °C for till), sliding stably as the temperature warms above and stick-slipping again when frozen below these estimated temperatures. Although the different bed types exhibit stick-slip behaviors at similar conditions, the mechanics of their drag are very different, demonstrated by friction that evolves over an order of magnitude more distance (D_c), significantly more rate-weakening ($b - a$), higher friction, and healing rates in frozen till compared to rock beds [Saltiel et al., 2021]. Resultant emissions have subtle differences, difficult to decipher visually, but which ML-based classification was able to identify; successfully predicting the bed type of a given waveform about 65% to 80% of the time, depending on the classification algorithm, processing steps, and data type used. The Random Forest Classifier was particularly successful (~77% mean prediction accuracy) and interpretable, since it provides feature importance of each waveform sample or frequency, showing the models focus on the initial wave arrivals and certain frequencies, where till events are higher amplitude. This is consistent with till's more impulsive failure, higher stress-drops, and friction, in turn due to a rougher and faster healing interface.

Given how different the slip mechanics of these two beds are, it is somewhat surprising how similar the resultant AEs are, but the interpretability of our ML results offers a path forward for classification. The findings are also counter to our original hypothesis based on the much longer frictional evolution distances (D_c) found in velocity-step experiments, which suggest less impulsive, lower frequency emissions. It is likely that different aspects of the frictional mechanics counter each other, for example more healing has been associated with higher frequency emissions in laboratory and natural faults [McLaskey et al., 2012], which could cancel the spectral effect of longer D_c. In a similar way, till experiments' higher D_c and $b - a$ balance each other to produce a critical rheological stiffness of the same order as rock [Saltiel et al., 2021]. In the end, our findings suggest that supervised ML-based classification and unsupervised correlation studies could find unknown and non-intuitive relationships between seismic emission characteristics and the mechanics / conditions of rupture in subglacial, as well as tectonic, volcanic, or induced seismicity settings. Laboratory experiments offer the opportunity to obtain well-controlled, labeled datasets, but results need to interpretable. Although it will be difficult to transfer models trained in the lab directly to field-scale data, the understanding gained can be used to infer characteristics of natural seismic sources.

Acknowledgments, Samples, and Data

S. Saltiel acknowledges the support of the Lamont-Doherty Postdoctoral Fellowship in Earth and Environmental Sciences. This research and S. Saltiel and C. McCarthy were funded by National Science Foundation (NSF)-1854629. Many thanks to T. Mittal for data processing and ML analysis suggestions, J. Tielke and T. Koczynski for laboratory assistance, as well as C. Marone, J. Rivière, and the Penn State Rock and Sediment Mechanics Lab for experimental acoustics advice.

Open Research

The datasets generated for this study are available on figshare.com at doi: 10.6084/m9.figshare.21257730, and Jupyter notebook for processing data is available at https://github.com/StraboAI/IcesAEs.

References

Aster, R. C., & Winberry, J. P. 2017. Glacial seismology. *Reports on Progress in Physics*, **80**, 126801. doi:10.1088/1361-6633/aa8473

Bougamont, M., Christoffersen, P., Price, S. F., Fricker, H. A., Tulaczyk, S., & Carter, S. P. 2015. Reactivation of Kamb Ice Stream tributaries triggers century-scale reorganization of Siple Coast ice flow in West Antarctica. *Geophysical Research Letters*, **42**(20), 8471-8480.

Breiman, L. 2001. Random Forests. *Machine Learning* **45**, 5–32 doi:10.1023/A:1010933404324

Clarke, G. K. 2005. Subglacial processes. *Annual Review of Earth and Planetary Sciences*, **33**(1), 247-276.

Cole, D. M. 1979. Preparation of polycrystalline ice specimens for laboratory experiments, *Cold Reg. Sci. Technol.*, 1, 153–159, doi: 10.1016/0165-232X(79)90007-7.

Cuffey, K.M. & Paterson, W.S.B., 2010. The Physics of Glaciers, 4th ed, Elsevier

Gräff, D., Köpfli, M., Lipovsky, B. P., Selvadurai, P. A., Farinotti, D., & Walter, F., 2021. Fine structure of microseismic glacial stick-slip. *Geophysical Research Letters*, **48**, e2021GL096043. https://doi. org/10.1029/2021GL096043

Gräff, D., & Walter, F., 2021. Changing friction at the base of an Alpine glacier. *Sci. Rep.* **11**, 10872. https://doi.org/10.1038/s41598-021-90176-9

Guerin, G., Mordret, A., Rivet, D., Lipovsky, B. P., & Minchew, B. M., 2021. Frictional origin of slip events of the Whillans Ice Stream, Antarctica. *Geophysical Research Letters*, **48**(11), e2021GL092950.

Iverson, N.R., 2010. Shear resistance and continuity of subglacial till: hydrology rules. *Journal of Glaciology*, **56** (200) 1104-1114. doi:10.3189/002214311796406220.

Hudson, T., Kufner, S. K., Brisbourne, A., Kendall, M., Smith, A., Alley, R., ... & Murray, T. 2022. Friction and slip measured at the bed of an Antarctic ice stream., Preprint from *Research Square*, DOI: 10.21203/rs.3.rs-1214097/v1

Kufner, S.-K., Brisbourne, A. M., Smith, A. M., Hudson, T. S., Murray, T., Schlegel, R., et al. 2021. Not all icequakes are created equal: Basal icequakes suggest diverse bed deformation mechanisms at Rutford Ice Stream, West Antarctica. *Journal of Geophysical Research: Earth Surface,* 126, e2020JF006001. Doi:10.1029/2020JF006001

Lipovsky, B.P., Meyer, C.R., Zoet, L.K., McCarthy, C., Hansen, D.D., Rempel, A.W. & Gimbert, F., 2019. Glacier sliding, seismicity and sediment entrainment. *Annals of Glaciology*, **60**(79), pp.182-192.

Marone, C., 1998. Laboratory-derived friction laws and their application to seismic faulting, *Ann. Rev. Earth Planet. Sci.*, **26**, 1, 643–696.

McCarthy, C., Savage, H.M., Koczynski, T., & Nielson, M.A., 2016. An apparatus to measure frictional, anelastic, and viscous behavior in ice at temperate and planetary conditions. *Review of Scientific Instruments*, **87**.

McCarthy, C., Savage, H.M., & Nettles, M., 2017. Temperature dependence of ice-on-rock friction at realistic glacier conditions, *Phil. Trans. R. Soc. A*, **375** (2086), 20150348.

McLaskey, G. C., Thomas, A. M., Glaser, S. D., & Nadeau, R. M., 2012. Fault healing promotes high-frequency earthquakes in laboratory experiments and on natural faults. *Nature*, **491**(7422), 101-104.

Nolte, D. D., & Pyrak-Nolte, L. J., 2022. Monitoring fracture saturation with internal seismic sources and twin neural networks. *Journal of Geophysical Research: Solid Earth*, **127**(2), e2021JB023005.

Parizek, B. R., Christianson, K., Anandakrishnan, S., Alley, R. B., Walker, R. T., Edwards, R. A., Wolfe, D. S., Bertini, G. T., Rinehart, S.K., Bindschandler, R. A., & Nowicki, S. M. J., 2013. Dynamic (in) stability of Thwaites Glacier, West Antarctica. *Journal of Geophysical Research: Earth Surface*, **118**(2), 638-655.

Rice, J. R., N. Lapusta, & Ranjith K., 2001. Rate and state dependent friction and the stability of sliding between elastically deformable solids, *J. Mech. Phys. Solids*, **49**, no. 9, 1865–1898.

Robin, G. de.Q. 1976. Is the Basal Ice of a Temperate Glacier at the Pressure Melting Point? *Journal of Glaciology*, **16**(74), 183-196. doi:10.3189/S002214300003152X.

Saltiel, S., McCarthy, C., Creyts, T. T., & Savage, H. M., 2021. Experimental evidence of velocity-weakening friction during ice slip over frozen till: Implications for basal seismicity in fast moving, soft-bed glaciers and ice streams. *Seismological Research Letters*, **92**(5), 2793-2810.

Schoof, C. 2005. The effect of cavitation on glacier sliding. *Proceedings of the Royal Society A: Mathematical, Physical and Engineering Sciences*. 461.2055. 609-627.

Schulson, E. M., & Fortt, A. L. 2012. Friction of ice on ice. *Journal of Geophysical Research: Solid Earth*, **117**(B12).

Thomason, J.F. & Iverson, N.R., 2008. A laboratory study of particle ploughing and pore-pressure feedback: a velocity-weakening mechanism for soft glacier beds. *Journal of Glaciology*, **54**(184), pp.169-181.

Wang, K., Johnson, C. W., Bennett, K. C., & Johnson, P. A., 2021. Predicting fault slip via transfer learning. *Nature communications*, **12**(1), 1-11. Doi: 10.1038/s41467-021-27553-5

Zoet, L. K., Anandakrishnan, S., Alley, R. B., Nyblade, A. A. & Wiens, D. A., 2012. Motion of an Antarctic glacier by repeated tidally modulated earthquakes. *Nature Geoscience*, **5**, 623-626.

Zoet, L.K., Carpenter, B., Scuderi, M., Alley, R.B., Anandakrishnan, S., Marone, C., Jackson, M., 2013. The effects of entrained debris on the basal sliding stability of a glacier. *Journal of Geophysical Research: Earth Surface*, **118**, 656-666.

Zoet, L.K., & Iverson, N.R., 2016. Rate-weakening drag during glacier sliding. *Journal of Geophysical Research: Earth Surface*, **121**(7), 1206-1217.

Zoet, L.K. & Iverson, N.R., 2018. A healing mechanism for stick-slip of glaciers. *Geology*, **46**(9), pp.807-810.

Zoet, L.K. & Iverson, N.R., 2020. A slip law for glaciers on deformable beds. *Science*, **368**(6486), pp.76-78.

Zoet, L.K., Ikari, M.J., Alley, R.B., Marone, C., Anandakrishnan, S., Carpenter, B.M., & Scuderi, M.M., 2020. Application of constitutive friction laws to glacier seismicity. *Geophysical Research Letters*, **47**(21), e2020GL088964.

[Geophysical Research Letters]

Supporting Information for

Characterization of Seismicity from Different Glacial Bed Types: Machine Learning Classification of Laboratory Stick-Slip Acoustic Emissions

S. Saltiel[1], N. Groebner[2], T. Sawi[3], C. McCarthy[3], B.K. Holtzman[3]

[1] Nevada Seismological Laboratory, University of Nevada, Reno, NV, USA

[2] Strabo Analytics, Inc, New York, NY, USA.

[3] Lamont-Doherty Earth Observatory, The Earth Institute, Columbia University of New York, NY, USA

Corresponding author: Seth Saltiel (ssaltiel@unr.edu)

Contents of this file

Text S1 to S5

Additional Supporting Information (Files uploaded separately)

Captions for Movie S1

Introduction

Supporting information of additional details on experimental methods and materials, as well as data processing. Text S1 includes details of ice, rock, and till sources and preparation procedures; apparatus design; and experimental protocols. Text S2 includes data cleaning and normalization processing steps. Dataset S1 is a movie of the experiment and data stream in real-time, including audible stick-slips that are simultaneous with AEs and mechanical stress-drops being recorded. The datasets generated for this study are available on figshare.com at doi: 10.6084/m9.figshare.21257730, and Jupyter notebook for processing data is available at https://github.com/StraboAI/IcesAEs.

Text S1: Experimental Details

For this study we only used bulk ice samples, frozen slowly from deionized water in a slightly oversized die, and subsequently cut down to 50 x 50 x 100 mm with a microtome housed in a cold room (~ - 12 °C). The bulk freezing process results in large, non-uniform grain size compared to 'standard ice,' created using a narrow range of seed ice grain sizes [Cole 1979]. Saltiel et al., [2021] showed an insignificant frictional difference between the two types, so we employed bulk ice in this study. The simplified freezing process is much less time intensive and allows the ultrasonic transducers to be frozen directly into the ice sample (Figure S1), minimizing travel distance from the ice-bed interface and contact surfaces which can greatly diminish recorded acoustic amplitudes. The sliding surfaces were roughened with a no. 100 grit sandpaper using the same procedure as McCarthy et al., [2017], who determined a roughness average (Ra) of 7 ± 1 μm using a profilometer (Mitutoyo SF-210).

Figure S1: Bulk ice with an ultrasonic transducer (AE sensor) frozen into it. The bulk freezing process allows the suspension of the sensor in the deionized water during slow freezing. The sensor is oriented to face the sides of the block, where the ice-bed interface, source of AEs, will be when loaded into the apparatus.

As in Saltiel et al., [2021], we control temperature with Peltier thermoelectric coolers in front and behind the ice block, as well as circulation of chiller fluid through the side blocks where both temperature and flow rate of chiller fluid were actively controlled to reach the desired temperature. Resistance Temperature Detectors (RTDs) ported directly behind the till or rock monitor the temperature as close to the sliding interfaces as possible. Unlike in Saltiel et al., [2021], we preformed experiments with both stable and changing temperature to explore the effect on stick-slip instability, stress-drops, and resulting AEs.

Actively chilled aluminum side blocks were employed with either frozen till or rock attached to their ice-facing sides (Figures 1a, S2). All till experiments used a sample collected from the Matanuska glacier in south-central Alaska and were prepared using the same procedure described in Saltiel et al., [2021]. For rock beds, we employed Barre granite quarried from Barre Township, Vermont, that was cut into two 10 x 50 x 50 mm slabs. A hole was drilled into the back side of the rock with the size and orientation of the side blocks' RTD port, to embed the RTD and measure the temperature directly behind the ice-rock interface. These slabs were then epoxied onto the aluminum side blocks and roughened using no. 100 grit sandpaper.

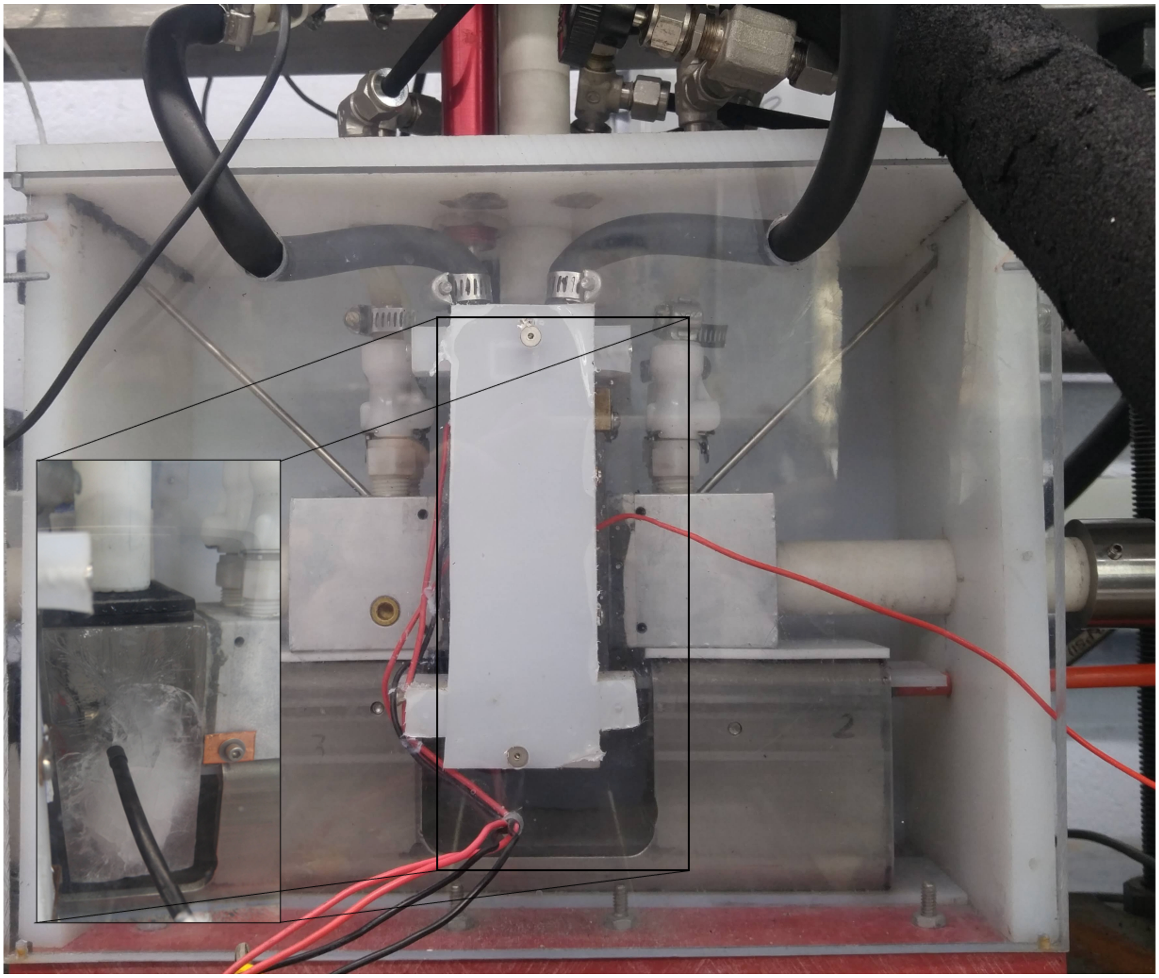

Figure S2: Photo of apparatus fully loaded. Since the peltier coolers cover the ice block, a photo without the cover is inset in the bottom left corner showing the central ice block at the end of an experiment, at the end of its full displacement.

All experiments were undertaken at ~50 kPa of normal stress and a load point velocity of 100 µm/s (just over 3 km/yr) for the entire displacement of 40 mm. This relatively high load point velocity was chosen because previous work has shown that stability decreases with slip velocity [Zoet et al., 2013, Saltiel et al., 2021]. Since the load point Linear Variable Differential Transformer (LVDT) only has 20 mm of stroke, the load point was stopped halfway through each experiment and then LVDT was reset to complete the rest of the experimental displacement. In this way, every experiment included a hold of about 60 seconds during which the shear stress relaxed and then reloaded, usually resulting in the largest stress-drop and AE of each experiment.

Text S2: Data Cleaning, Trimming, and Normalization

We implemented a data cleaning, trimming, and normalization approach based on that implemented by Nolte and Pyrak-Nolte [2022]. First, waveforms were trimmed to a total of 1200 samples, including 400 samples before the trigger point, giving a total window of 15 microseconds. Waveforms were then normalized by the sum of the squared amplitudes of the first 400 samples after the trigger, multiplied by a cosine taper. Zero and large amplitude waveforms were removed, defined as having a sum of the first 400 normalized samples greater than 15. This threshold was found to give the best catalog of non-noise events without removing too many. 325 events were then removed that a have high amplitude low frequency noise component. Finally, the waveforms were realigned to the first maximum peak after the trigger, which refined alignment by a few samples in most cases. From this catalog of normalized, filtered, and aligned 1200-sample waveforms, we used a trial-and-error approach to determine how much of the pre- and post-trigger waveforms to use for training the models and found a total length of 150 samples, with 45 before the trigger, was optimal. This subsample of the waveforms emphasizes the first arrivals of each AE, which are more dependent on source effects, while ignoring the coda, which depend more on path effects. Although, as we will show in the next section, the original, unprocessed catalog was able to produce as high prediction accuracies, the processed waveforms were clearer to interpret, the main point of this study.

Text S3: Results from Suite of ML Classification Algorithms

We systematically tested of a suite of ML classification algorithms, the original, full catalog and that created by the trimming and cleaning processing steps described above, using both waveforms and spectra. Figures S3 – S6 show the distributions of prediction accuracies for each of these combinations of algorithms and catalogs.

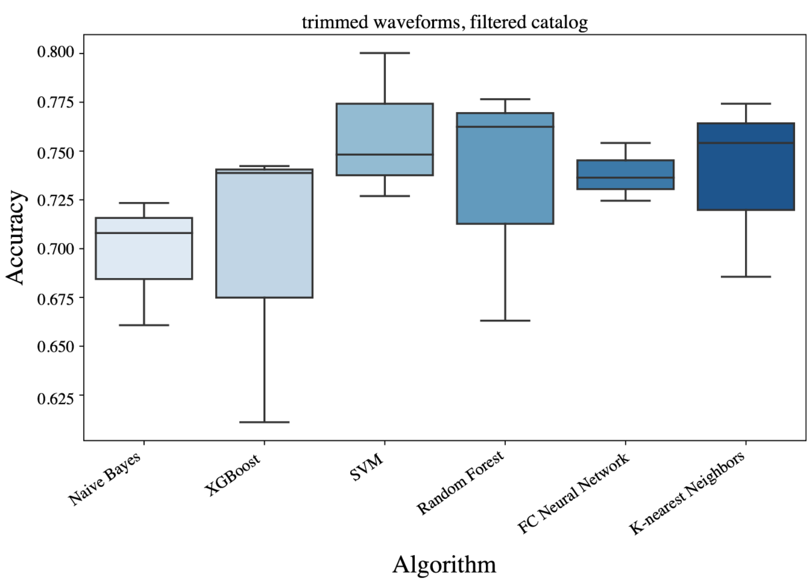

Figure S3: Whisker plot showing the distribution of prediction accuracies using the processed waveform catalog for each algorithm tested. Random Forest Classifier shows the highest mean accuracy of the all the algorithms which give a distribution, and, most importantly, provides feature importance for interpretation, so we focus on those results.

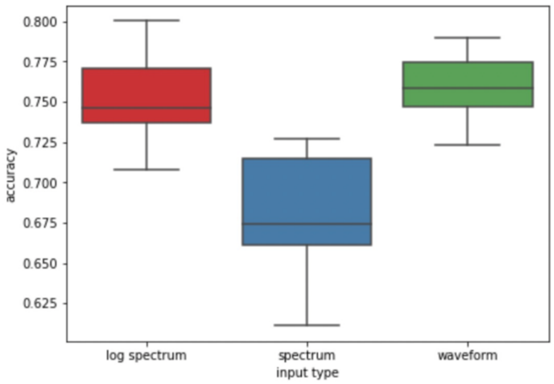

Figure S4: Whisker plot showing the distribution of prediction accuracies for each input data type tested, using the processed catalog. Waveforms show the tightest distribution and highest mean. Spectra are not very accurate, because the low frequency power dominates the spectral power and thus contains little information (see S4 below). But $\log_{10}$ of the spectrum retain the high frequency information and accuracy can be as high as the predictions using waveforms.

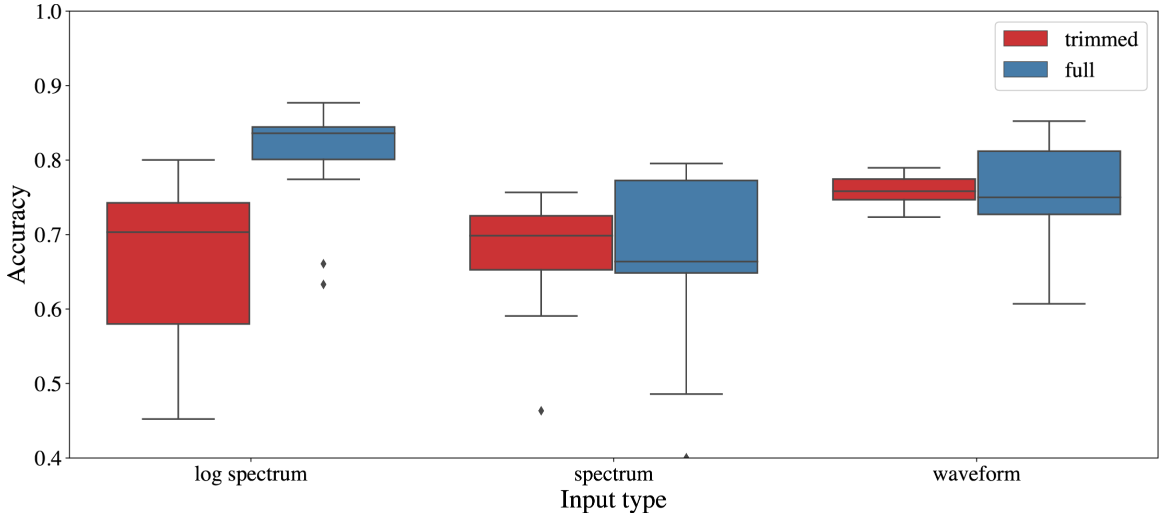

Figure S5: Whisker plot showing the distribution of prediction accuracies for the original, ‘full’, catalog of events vs. the processed, ‘trimmed’, catalog, using the processing steps described in text S2. Although the full catalog is able to give as good, or sometimes better predictions accuracies, which is not surprising since it contains more information, we focus our analysis on the processed, ‘trimmed’, catalog since the results are easier to interpret, the main focus of this study.

Text S4: Predictions using Spectrum vs Log Spectrum

We first undertook our analysis using spectrum, to test the predictive power of spectral information. But since the low frequency power dominates, using straight spectral power greatly diminishes the amount of data available (Figure S6a), and thus the predictions are relatively poor (Figure S4). By taking the log of the spectrum the higher frequency information is useful (Figure S6b) and predictions are more accurate.

a)

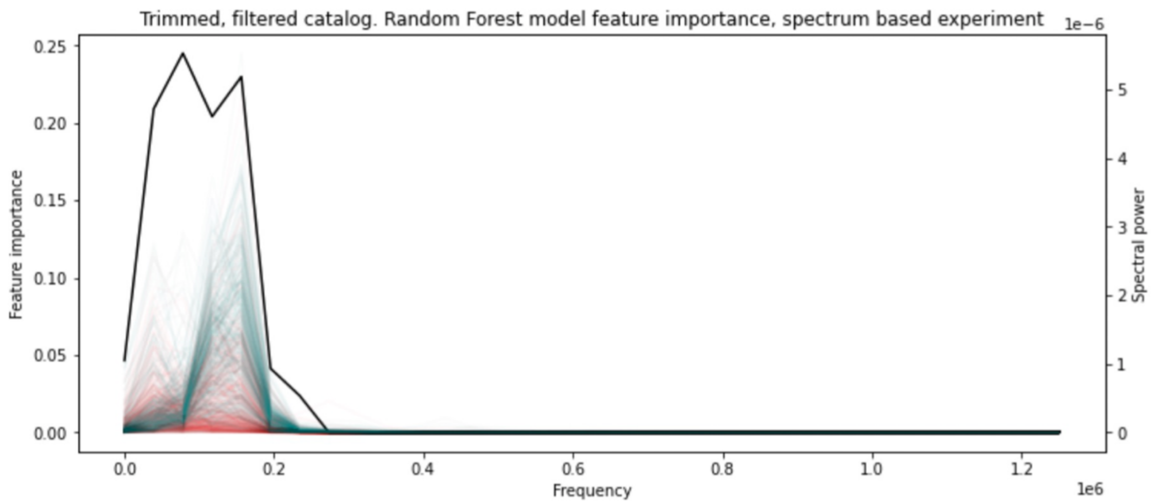

b)

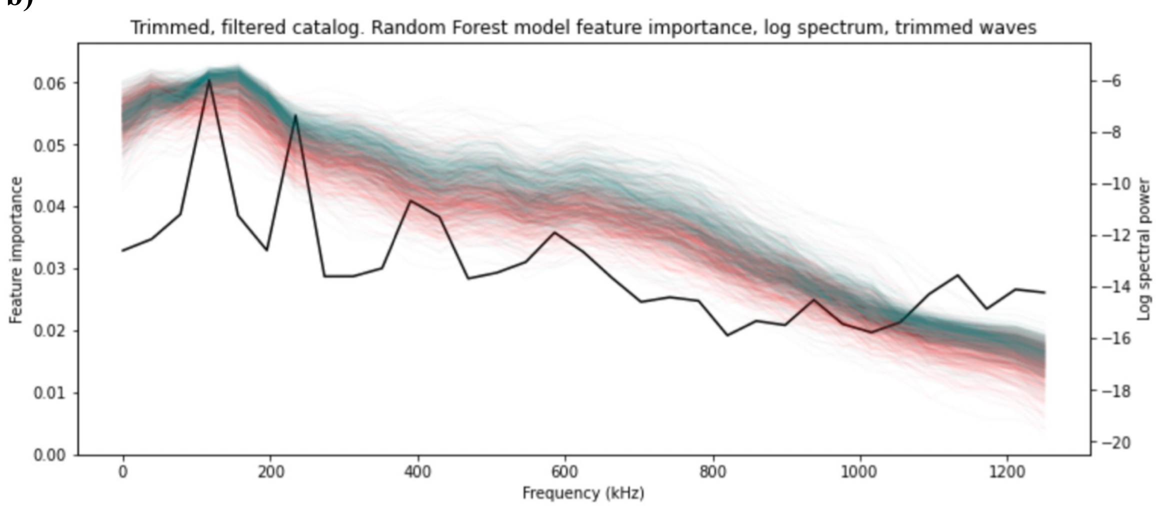

Figure S6: a) Spectrum from every till (teal) and rock (red) event, and the feature importance used to make Random Forest Classifier model predictions. Most spectral power is below 200 kHz, **b)** by taking the log spectrum, the higher frequency information is useable and prediction accuracy is improved.

Text S5: Testing Experimental Differences

To ensure that the prediction is not based on some aspect of the waveform specific to the ice sample or other uncontrolled aspect of the experiment and not the bed type which we are testing for, we also tested each experiment independently, not allowing the algorithm to train on data from the same experiment as the testing. We divide the data into training and test sets based on experiment, i.e., for a given model training run the waveforms from 5 till and 5 rock experiments are used for the training set, and the remaining 1 till and 1 rock experiment are used for testing. By separating training and test sets by experiment, any experiment-dependent features of the waveforms would be irrelevant for classification. The prediction accuracy is summarized by a 6 till by 6 rock experiments matrix, giving the accuracy for 36 models with each combination used as the testing data (Figure S7).

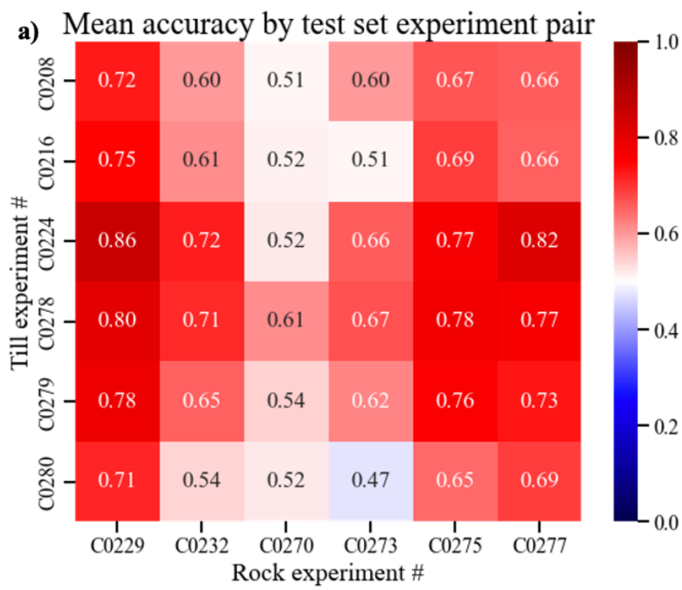

b)

Exp. (C0#)	Bed type	Temp (~°C)	# of events	Accu -racy
208	Till	-3	94	67%
216	Till	-3	465	71%
224	Till	-2.5	245	86%
278	Till	-3.4	421	82%
279	Till	-4	181	74%
280	Till	-4	141	63%
229	Rock	-6 => -4	319	82%
232	Rock	-4 => -3	184	51%
270	Rock	-3	296	38%
273	Rock	-3.8	95	42%
275	Rock	-4.3 => -3.9	150	71%
277	Rock	-3.9	226	68%

Figure S7: a) Mean prediction accuracy given different sets of rock and till experiments used as testing dataset. In each case, the other experiments were used as training data, producing a model for each combination of testing experiments (6 till and 6 rock experiments make for 36 different train and test datasets, and models). Although some experimental variation is expected, relatively consistent results across testing datasets (either randomly selected from all experiments or from an individual one) shows that the overall predictability is not experiment dependent. **b)** Table on right provides the temperature range, number of events, and accuracy for each individual experiment.

This prediction accuracy calculates how often the model could correctly classify individual waveforms as coming from till or rock beds, but we envision a tool whereby a collection of seismic events recorded from a given location would be analyzed to determine the probability it came from a till- or rock-bedded section of a glacier. So, the more relevant accuracy is if a single experiment can be accurately predicted to be till or rock, and how many events would be needed to make such a prediction accurate. Since its clear from Figure 5 that there are overlapping ‘till-like’ rock events and visa-versa, the direct prediction does not have to be used for the overall population prediction. For example, we find that all the experiments can be correctly predicted if 37.5% ‘rock-like’ events, or 62.5% ‘till-like’ events, is used as the cut-off for overall prediction (Figure S8). Our data shows a sharp cut off at these values, so it likely would not remain a perfect classifier with more experiments, but it does suggest how predictions might be made given the overlapping event populations.

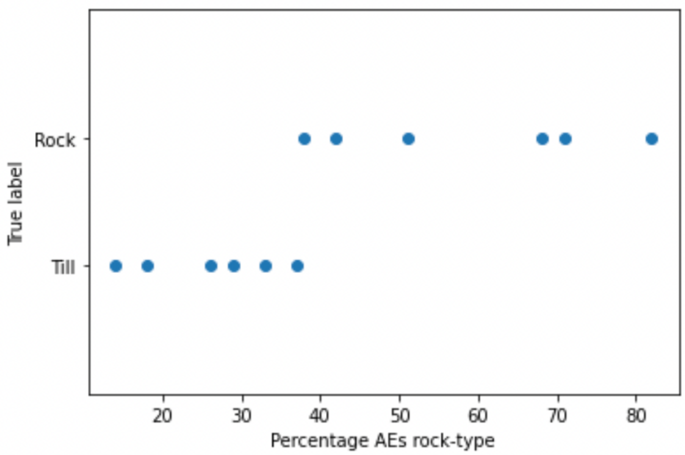

Figure S8: Each experiments percentage of events predicted as rock, which we label as ‘rock-like’ events. The till and rock experiments perfectly separate if more than 37.5% of the events are predicted as rock.

Since there are rock experiments with more ‘till-like’ events than ‘rock-like’ events, it is possible that the model is ‘defaulting’ to till since there are slightly more till than rock events overall. We do not believe this is the case, given the significant overlap in the characteristics of rock and till events (Figure 5). While the rock stress-drops have a tighter distribution (Figure 4c), these stress drops do not follow a simple relationship with recurrence interval, as would be expected with a single healing rate and as seen with the till experiments (Figure 4d). Although there is not enough data to fully constrain, Figure 4d suggests that some rock experiments sit on the till healing relation (stress-drops of about 25 kPa per second of recurrence interval), while others have lower healing rates. This may explain the imbalance in prediction accuracy, why there are more ‘till-like’ rock AEs than ‘rock-like’ till AEs. Some experiments near the cut-off, such as 270, would be very difficult to predict correctly. 270 is one of the rock experiments with a high healing rate (~22 kPa/s), which might contribute to its having more ‘till-like’, misclassified events.

Movie S1: Movie of experiment and AE recording in real-time. Audible stick-slips and mechanical stress-drop data (not shown) both simultaneously occur with the recorded AEs. Some events appear to have two arrivals, probably one from each ice interface, since they have different path lengths they arrive at the sensor at slightly different times even if they occur at the same time. In these cases, the processing steps from text S2 remove the later arrival.